Deactivation Behavior of Carbon Nanotubes Supported Cobalt Catalysts in Fischer-Tropsch Synthesis

Trépanier, Mariane
Department of Chemical Engineering, University of Saskatchewan, Saskatoon, SK, S7N5C5 CANADA

Tavasoli, Ahmad*+; Anahid, Sanaz
School of Chemistry, College of Science, University of Tehran, Tehran, I.R. IRAN

K. Dalai, Ajay
Department of Chemical Engineering, University of Saskatchewan, Saskatoon, SK, S7N5C5 CANADA

ABSTRACT: *The effects of electronic properties of inner and outer surfaces of Carbon Nano Tubes (CNTs) on the deactivation of cobalt Fischer-Tropsch (FT) catalysts were studied. The comparative characterization of the fresh and used catalysts by TEM, XRD, TPR, BET and H_2 chemisorption showed that cobalt re-oxidation, cobalt-support interactions and sintering are the main sources of catalyst deactivation. TEM showed that 480 h continuous FT synthesis increased the average particles size of the particles located inside the pores from 7 to 7.4 nm while the average particles size of the particles located outside of the tubes increased from 11.5 to 25 nm. XRD analysis of the used catalyst confirmed cobalt re-oxidation and interaction between cobalt and CNTs and creation of carbide phases. When the %Co conversion and H_2O partial pressure in the reactor are high, the deactivation rate is not dependent on the number of the catalyst active sites and is zero order to %CO conversion. In this case the main deactivation mechanisms are cobalt re-oxidation and metal support interactions. At lower amounts of the %Co conversion and H_2O partial pressure, deactivation can be simulated with power law expressions with power orders of 11.4 for the particles outside the tubes and 30.2 for the particles inside the tubes and the main deactivation mechanism is sintering. Due to the electron deficiency of the inner sides of the CNTs, the interaction between the cobalt oxides and the support is stronger leading to lower rates of sintering as compared with the particles located on the outer layers of the CNTs. Regeneration recovered the catalyst activity by 54.3% of the total activity loss.*

KEY WORDS: *Fischer-Tropsch, Cobalt, Carbon nanotubes, Deactivation, Sintering.*

INTRODUCTION

Fischer-Tropsch Synthesis (FTS) is a potentially promising option for environmentally friendly production of chemicals and fuels from biomass, coal and natural gas [1-2]. In industrial applications, a high-performance catalyst plays

* *To whom correspondence should be addressed.*
+ *E-mail: tavassolia@khayam.ut.ac.ir*
1021-9986/11/1/37 11/$/3.10

an essential role. In FTS process, the catalyst activity, selectivity and lifetime are influenced by nature and structure of support, nature of metal, metal dispersion, metal loading, and catalyst preparation method [3-4]. Most studies on FTS catalysts have been carried out with the metals supported on silica, alumina or titania. In addition, other families of supports with carbonaceous base such as activated carbon have been investigated for FT reactions [5-13]. Activated carbon has many advantages if utilized as FTS catalyst support (resistance to acidic or basic media, stable at high temperatures, etc.). Carbon Nano Tubes (CNTs) possess similar properties and in most cases outperform activated carbon in this respect [14]. Carbon nanotubes with unique properties such as uniform pore size distribution, meso and macro pore structure, inert surface properties, and resistance to acid and base environment can play an important role in a large number of catalytic reactions [13]. In our previous works [5-9] we reported on the interesting catalytic properties of CNTs supported cobalt catalysts prepared by the sequential aqueous incipient wetness impregnation method. We showed that from a catalytic activity standpoint, the FT synthesis rate and percentage CO conversion obtained by carbon nanotubes supported cobalt catalysts were 50-75% higher than that obtained with alumina supported cobalt catalysts with the same cobalt loading in both fixed bed and slurry reactors. Also CNTs caused a slight decrease in the FTS product distribution to lower molecular weight hydrocarbons, requiring smaller hydro-cracker in the product upgrading section.

While Co/CNTs catalyzed FT synthesis is advantageous in carbon utilization as compared to processes using Co/Al_2O_3, Co/SiO_2 or Co/TiO_2 catalysts, CNTs supported cobalt catalysts are more expensive necessitating longer catalyst life [5-9]. Catalyst stability therefore is an important performance variable in Co/CNTs catalyzed FT process. In the case of silica, alumina and titania supported cobalt catalysts, the potential causes of cobalt FTS catalyst deactivation include (a) oxidation of the cobalt surface, (b) cobalt support interactions and formation of mixed compounds that are reducible only at high reduction temperatures, (c) sintering, (d) refractory coke formation, (e) loss of metal cobalt because of attrition and (f) heteroatoms poisoning (i.e. sulphur) [15-17].

In the present work, the deactivation properties of CNTs supported cobalt catalyst during 480 h continues FT synthesis in a fixed bed micro reactor was investigated considering different deactivation mechanisms. The main objective of the current work is to study the effect of electronic properties of the inner and outer surfaces of the carbon nanotubes on the deactivation of Co/CNTs catalysts.

EXPERIMENTAL SECTION

Catalyst preparation

Purified Multi-Wall Carbon Nano Tubes (MWCNT) were used as support material for the preparation of FTS catalyst. Prior to impregnation, the support was treated with 30 wt% HNO_3 at 100°C over night, washed with distilled water, and dried at 120°C for 6 h. The purified CNTs were loaded with 20 wt% cobalt using sequential incipient wetness impregnation of cobalt nitrate ($Co(NO_3)_2.6H_2O$ 99.0%, Merck) solution. After each impregnation step, the catalyst was dried at 120°C for 6 h and calcined at 350°C for 3h at a heating rate of 10°C/min under argon flow.

ICP

The cobalt loadings of the calcined fresh and used catalysts were verified by an Inductively Coupled Plasma Atomic Emission Spectroscopy (ICP-AES) system.

Transmission Electron Microscopy (TEM)

The morphology of the support, fresh and used catalysts was studied by transmission electron microscopy. Sample specimens for TEM studies were prepared by ultrasonic dispersion of the catalysts in ethanol, and the suspensions were dropped onto a copper grid. TEM investigations were carried out using a Hitachi H-7500 (120kV). Several TEM micrographs were recorded for each sample and analyzed to determine the particle size distribution.

Scanning Electron Microscopy (SEM)

The samples were characterized by scanning electron microscopy. SEM analysis was carried out using a Hitachi S-4700 at 3 kV. Sample specimens for SEM were prepared by ultrasonic dispersion of samples in methanol. The suspensions were dropped onto a carbon support cover with a thin silica layer which allows seeing carbon nanotubes at high resolution.

BET surface area measurements/ pore size distributions

The surface area, pore volume, and average pore radius of the support; fresh and used catalysts were measured by an ASAP-2010 system from Micromeritics. The samples were degassed at 200°C for 4 h under 50 mTorr vacuum and their BET area, pore volume, and average pore radius were determined.

ray diffraction

XRD measurements of the support, fresh and used catalysts were conducted with a Philips PW1840 X-ray diffractometer with monochromatized Cu/K_α radiation. Using the Scherrer equation, the average size of the cobalt oxide crystallites in the calcined fresh and used catalysts were estimated from the line broadening of the cobalt oxide peaks.

Temperature programmed reduction

Temperature Programmed Reduction (TPR) spectra of the fresh and used catalysts were recorded using a Micromeritics TPD-TPR 290 system, equipped with a thermal conductivity detector. The catalyst samples were first purged in a flow of argon at 100°C, to remove traces of water, and then cooled to 40°C. The TPR of 50 mg of each sample was performed using 5.1% hydrogen in argon gas mixture with a flow rate of 40 cm^3/min. The samples were heated from 40 to 900°C with a heating rate of 10°C /min.

Hydrogen chemisorption and reoxidation

The amount of chemisorbed hydrogen on the fresh and used catalysts was measured using the Micromeritics TPD–TPR 290 system. 0.25 g of the sample was reduced under hydrogen flow at 400°C for 12 h and then cooled to 100°C under hydrogen flow. Then the flow of hydrogen was switched to argon at the same temperature, which lasted about 30min in order to remove the weakly adsorbed hydrogen. Afterwards, the Temperature Programmed Desorption (TPD) of the samples was obtained by increasing the temperature of the samples, with a ramp rate of 10 °C/min, to 400°C under the argon flow. The TPD spectrum was used to determine the cobalt dispersion and its surface average crystallite size. After the TPD of hydrogen, the sample was reoxidized at 400°C by pulses of 10% oxygen in helium to determine the extent of reduction. It is assumed that Co^o is oxidized to Co_3O_4. The calculations are summarized below [16,17].

$$\text{calibration value (l gas / area units)} = \frac{\text{loop volume} \times \%\text{analitical gas}}{\text{mean calibration area} \times 100} \quad (1)$$

$$H_2 \text{ uptake (moles / } g_{cat}) = \frac{\text{analitical area from TPD} \times \text{calibration value}}{\text{sample weight} \times 24.5} \quad (2)$$

$$\%D_{\text{TotalCo}} = \frac{H_2 \text{ uptake} \times \text{atomic weight} \times \text{stoichiometry}}{\%\text{metal}} = \frac{\text{number of Co}^o \text{ atoms on the surface} \times 100}{\text{total number of Co}^o \text{ atom}} \quad (3)$$

$$\%D_{\text{reducedCo}} = \frac{\text{number of Co}^o \text{ atoms on the surface} \times 100}{\text{total number of Co}^o \text{ atom} \times \text{fraction reduced}} \quad (4)$$

$$O_2 \text{ uptake (moles / } g_{cat}) = \frac{\text{sum of consumed pulses areas} \times \text{calibration value}}{\text{sample weight} \times 24.5} \quad (5)$$

$$\text{Fraction reduced} = \frac{O_2 \text{ uptake (moles / g.cat.)} \times 2/3 \times \text{atomic weight}}{\text{Percentage metal}} \quad (6)$$

$$\text{Diameter(nm)}_{\text{totalCo}} = \frac{6000}{\text{density} \times \text{maximum area} \times \text{dispersion}} \quad (7)$$

$$\text{Diameter(nm)}_{\text{reducedCo}} = \frac{6000}{\text{density} \times \text{maximum area} \times \text{dispersion} \times \text{Fraction reduced}} \quad (8)$$

Reaction setup and experimental outline

The catalyst was evaluated in terms of it's FTS activity (g HC produced/ g cat./ h) and selectivity (the percentage of the converted CO that appears as a hydrocarbon products) in a fixed bed micro-reactor. The temperature of the reactor was controlled via a PID temperature controller. Brooks 5850 mass flow controllers were used to add H_2, CO and argon at the desired rate to the reactor. Argon was used as internal

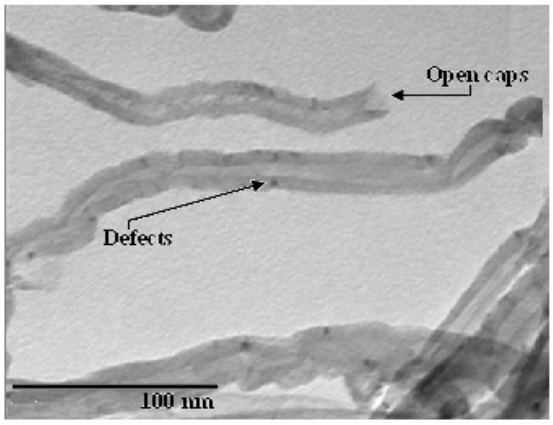

Fig. 1: TEM image of the CNTs as support material after treatment with acid.

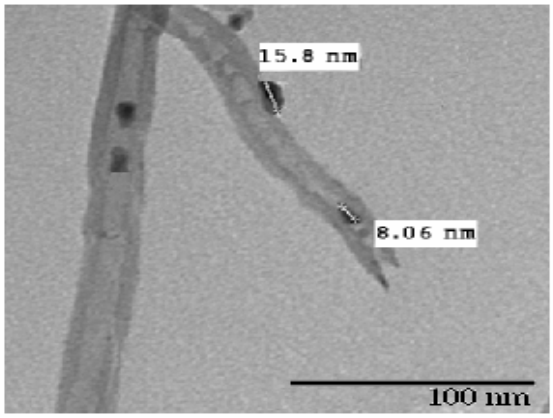

Fig. 2: TEM image of the calcined fresh catalyst: cobalt particles are uniformly distributed inside and outside of the tubes.

standard gas in the reactor feed. Prior to the activity tests, the catalyst activation was conducted according to the following procedure. The catalyst (1g) was placed in the reactor and pure hydrogen was introduced at a flow rate of 60 mL/min. The reactor temperature was increased from room temperature to 400°C at a rate of 10°C/min, maintained at this activation condition for 20 h and the catalyst was reduced in-situ. After the activation period, the reactor temperature was decreased to 180°C under flowing hydrogen.

The mixed gases entered through to the top of the fixed bed reactor. Synthesis gas with a flow rate of 45 mL /min (H_2/CO ratio of 2) was introduced and the reactor pressure was increased to 2 MPa. The reactor temperature was then increased to 220°C at a rate of 10°C /min. Products were continuously removed from the vapour and passed through two traps, one maintained at 100°C (hot trap) and the other at 0°C (cold trap). The uncondensed vapour stream was reduced to atmospheric pressure through a back pressure regulator. The composition of the outlet gas stream was determined using an on-line GC-2014 Shimadzu gas chromatograph. The contents of hot and cold traps were removed every 24 h analyzed by Varian 3400 GC gas chromatograph.

After 480 h of the first FT synthesis step, the flow of synthesis gas was switched off and catalyst was re-reduced (second treatment step) in a flow rate of 60 mL/min H_2 at 270°C for 20 h. Then the second FT synthesis step was carried out under the same conditions of the first synthesis step and the activity (g HC produced/ g cat/ min) and selectivity of the system were measured. The third treatment step of the catalyst was performed at 400°C for 20 h. Subsequently the reactor was cooled to 220°C and the third FT synthesis step was carried out under the same conditions of the previous synthesis steps. The products are analysed under the same conditions of the first synthesis step. Then the catalytic bed was washed by helium flow for 3 h at 270°C to remove the heavy waxes inside the catalyst pores. The temperature of the reactor was lowered to the 20°C and the catalyst was passivated with pulses of dry air. The used catalyst was discharged and characterized extensively.

RESULTS AND DISCUSSION

Characterization overview

A sample of the purified CNTs material was analyzed by TEM. The purified product consisted of an interwoven matrix of tubes (Fig. 1) that was shown to be comprised of multi-walled carbon nanotubes. The TEM image of calcined fresh catalyst revealed that the catalyst particles were well dispersed inside the tubes and also on the perimeter of the tube walls (Fig. 2). Dark spots represent the cobalt oxides which are attached inside or outside of the nanotubes. This figure shows that the majority of the cobalt particles (about 65-70%) are distributed in the inner pores of the CNTs. This can be attributed to carbon nanotubes tubular morphology which can induce capillary forces during the impregnation process. The particles measurement has been calculated using the following equation $d=(4\times a\times b/\pi)0.5$ where a and b are dimensions of the particles as seen in the TEM image. The cobalt oxide particles inside the CNTs are fairly

uniform in the fresh catalyst and the most abundant ones have sizes comprised in the 4-11 nm range. This is in accordance with the average inner diameter of the CNTs (12 nm), whereas those on the outer surface have grown to about 16 nm (Fig. 2). Obviously, the CNTs channels have restricted the growth of the particles inside the tubes. A bar graph depicting the size distribution of the total particles inside and outside the tubes determined from the particle size distribution of 10 TEM pictures is shown in Fig. 3. This figure shows that the average particles size for the particles located on the inner surface of the tubes is about 7 nm and that of the particles located on the outer surface of the tubes is about 11.5 nm.

In addition to the catalyst particles visible in Fig. 2, the representative SEM image of the fresh catalyst shown in Fig. 4 reveals the outside of CNTs walls. The SEM picture reveals that the support material is entirely comprised of nanotubes and there are no other impurities such as nanospheres.

Fig. 5 shows TEM picture of the used catalyst. As shown in this picture, there are still small particles (4-11 nm) inside the CNTs while the particles attached to the outer surfaces of the CNT have grown significantly (i.e. 40^{+}nm). The cobalt oxide particles inside the channels do not experience particle agglomeration significantly. This phenomenon can be related to the interaction of the metal site with the inner surface of the tubes and perhaps to the spatial restriction of the CNTs channels. However, most of the cobalt oxides on the exterior surface agglomerated resulted in lower metal site dispersion under FT reactions. Carbon nanotubes are different compared to other carbonaceous supports in that they have graphene layers with a tubular morphology. Theoretical studies reveal that deviation of the graphene layers from planarity causes π-electron density to shift from the concave inner surface to the convex outer surface, leading to an electron-deficient interior surface and an electron-enriched exterior surface [18-20]. This can influence the structure and electronic properties of substances in contact with either surface. It can be concluded that, due to the electron deficiency of the inner sides of the CNTs, the interaction between the cobalt oxides and the support could be stronger; thus leading to lower rates of sintering than that of the particles located on the outer layer of the CNTs. Also the particles inside the tubes are rather less mobile and consequently the sintering occurrence is considerably limited.

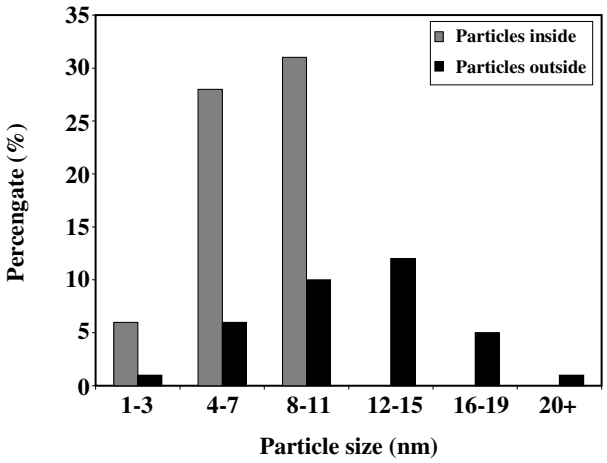

Fig. 3: Cobalt oxides particle size distribution for calcined fresh catalyst based on 10 TEM pictures

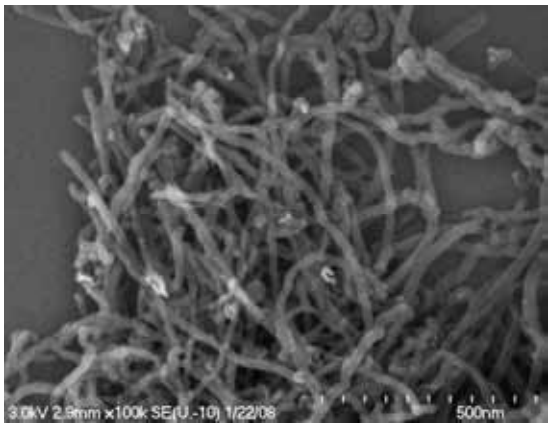

Fig. 4: SEM image of the calcined fresh catalyst.

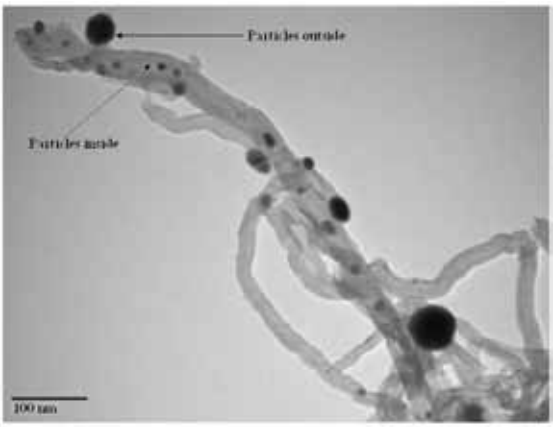

Fig. 5: TEM image of the used catalyst showing the cobalt particles outside and inside of the tubes..

Table 1: BET surface area, porosity, XRD and TPR data for the fresh and used catalysts.

Catalysts/ Support	ICP	BET (m^2/g)	Pore volume (cm^3/g)	Pore Radius (nm)	XRD d(nm)	1st TPR peak (°C)	2nd TPR peak (°C)
CNT	-	210	0.6	6.1	-	-	-
Fresh catalyst	19.8	163	0.47	5.8	8.5	330	428
Used Catalyst	19.7	121	0.36	5.9	17	270	380

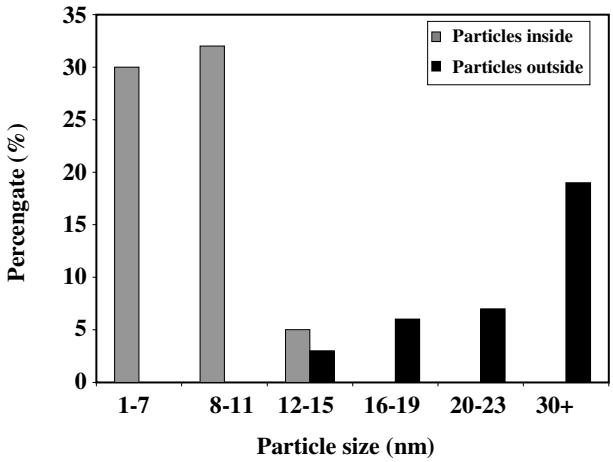

Fig. 6: Cobalt oxides particle size distribution for used catalyst based on 10 TEM pictures.

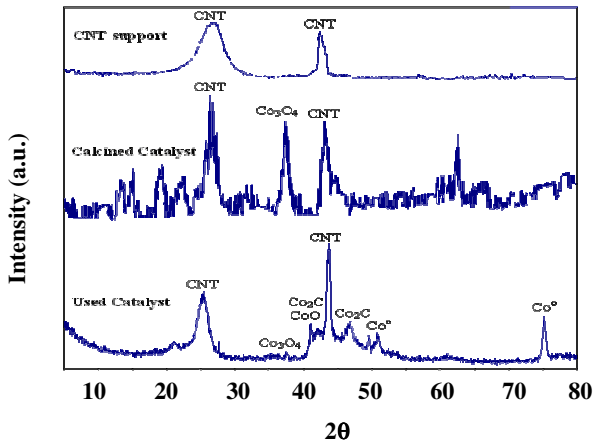

Fig. 7: XRD spectra for the pure CNTs, calcined fresh and used 20wt%Co/CNT catalysts.

A bar graph depicting the size distribution of the cobalt oxide particles inside and outside of the tubes determined from the particle size distribution of 10 TEM pictures for the used catalyst is presented in Fig. 6. Comparing Figs. 3 & 6, clearly show that the sintering rate of the particles located on the outer surface of the tubes is too high. However the sintering rate for the particles located on the inner surface of the tubes is not significant. In the case of the particles located on the inner surface of the tubes the average particles size increased from 7 to 7.4 nm and that of the particles located on the outer surface of the tubes increased from 11.5 to 25 nm.

Table 1 shows the metal content for the fresh calcined and used catalysts. ICP analyses of the catalysts revealed that the metal contents of the catalysts were fairly similar and close to the targeted metal content of 20 wt% Co. Table 1 also shows the results of surface area measurements of the purified CNTs and fresh and used catalysts. In the case of the fresh calcined catalyst, loading of 20% Co decreased the surface area from 210 to 163 m^2/g and the pore volume from 0.6 to 0.47 indicating pore blockage due to cobalt loading on the support. Table 1 shows that 480 h FT synthesis decreases the BET surface area of the catalyst from 163 to 121 m^2/g and the catalyst pore volume from 0.47 to 0.36 cm^3/g. Sintering of the particles and pore blockage during the FT synthesis are the main reasons of decrease in BET surface area and pore volume.

XRD profiles of the purified CNTs, fresh and used catalysts are shown in Fig. 7. For CNTs, calcined fresh and used catalysts, the peaks at 2θ of 25 and 43° correspond to graphite layers (multi wall carbon nanotubes), while the other peaks in the spectrum of fresh catalyst are related to different crystal planes of Co_3O_4. No peak was observed indicating formation of cobalt support compounds in the fresh catalyst XRD spectrum. In the XRD of the fresh catalyst the peak at 36.8° is the most intense peak of Co_3O_4. In the XRD spectrum of the used catalyst, the peak at 2θ value of 47° correlates well with Co_2C. Also the peaks at 2θ values of 51.1 and 75.8° are correspond to the metallic cobalt (Co^o) [21,22]. Also the small peaks at 2θ values of 36.8° and 42.5° correspond to Co_3O_4 and CoO [21,22]. The presence of Co_2C can be attributed to either a cobalt-CNTs interaction or a Co-carbon reaction during the carbon monoxide dissociative adsorption.

Table 2: %Dispersion and crystallite sizes of unreduced and reduced cobalt particles determined by H_2 TPD and pulse reoxidation of the fresh and used catalysts.

Catalysts	μ mole H_2 desorbed /g cat.	μ mole O_2 Consumed /g cat.	%Red.	%Dispersion (Tot. Co)	%Dispersion (Red. Co)	dp (nm) (Tot. Co)	dp (nm) (Red. Co)
Fresh catalyst	221.4	1602.2	63.9	10.4	16.3	9.9	6.3
Used Catalyst	178.9	1337.7	53.4	8.4	15.7	17.5	9.4

Although a fraction of cobalt clusters may oxidize in presence of significant amount of water formed during FT synthesis with high conversions, some amount of the cobalt oxide in the used sample probably is formed during the discharge and passivation step at room temperature. Table 1 shows the average cobalt oxide particle size of the fresh and used catalysts calculated from XRD spectrum and Scherrer equation. In accordance with the results of the TEM analyses, XRD results show that there is a significant particle growth in the course of FTS reaction. There is a good agreement between the data for average particle size calculated based on XRD and TEM size distribution.

The activation of the fresh and used catalysts in hydrogen atmosphere was disclosed by temperature programmed reduction (TPR) experiments. The TPR spectra of the fresh and used catalysts are shown in Fig. 8. In the profile of the fresh catalyst, the first peak at 330°C is typically assigned to the reduction of Co_3O_4 to CoO, although a fraction of the peak likely comprise the reduction of the larger, bulk-like CoO species to Co^o [21]. The second broader peak at 428°C, is mainly assigned to the second step reduction, which is mainly reduction of CoO to Co^o. The small peak at about 600°C in the TPR spectra of the fresh catalyst can be assigned to the gasification of support as indicated by TPR of pure CNT support at about 600^oC [22].

Fig. 8 also shows that, the peaks of the used calcined catalyst shifted to lower temperatures showing that the reduction of the cobalt oxides of the used calcined catalyst occurred at lower temperatures than that of the fresh calcined catalyst. According to the reduction peak temperatures (Table 1), 480 h FT synthesis results in a decrease in the temperature of the first TPR peak from 330 to 270^oC and that of the second TPR peak from 428 to 380^oC, suggesting an easier reduction process. This can be due to easier reduction of the larger cobalt particles as confirmed by the results of TEM and XRD tests or even to the presence of less stable oxides. However, the total H_2 consumption is lower in the case of the used catalyst; this is an indication of porosity decrease (Table 1) due to particle growth and differentiation of the cobalt species (i.e. carbides).

It has been shown that the interaction of the metal oxide nanoparticles with the inner and outer CNTs surfaces can affect the reduction behaviour of the metal oxides [18]. The electron deficiency of the interior CNT surface can facilitate the reduction of the metal oxides located in the inner surface of the tubes as compared with the particles located in the outer surface of the tubes [18]. Sintering of the particles attached to the outer surface of the tubes during FT synthesis (As confirmed by TEM pictures) increases the ratio of the numbers of the particles located inside to the number of the particles located on the outer surface of the tubes. In fact the ratio of the easily reducible particles to the total particles increases in the course of FT reaction. This can be another reason for lower TPR peak temperatures in the case of the used calcined catalyst.

The results of H_2 chemisorption and oxygen titration tests for the fresh and used catalysts are shown in Table 2. In accordance with the TPR results, the hydrogen consumption for the used catalyst is lower than that of the fresh calcined catalyst. %Reduction decreased by about 10% and %dispersion calculated based on the total cobalt and reduced cobalt decreased significantly. In agreement with the data obtained by TEM and XRD experiments, the particles diameters calculated based on the total cobalt and reduced cobalt increased significantly in the course of 480 continues FT synthesis.

Activity and products selectivities results

Table 3 presents the FT synthesis rate (g CH/g cat./h), %CO conversion, chain growth probability and different product selectivities during first 12 hours of FT synthesis. As shown in this Table the FT synthesis productivity of the 20wt.%Co/CNT catalyst (0.4192 g CH/g cat/h) is greater than that of the commercial Al_2O_3, SiO_2 and TiO_2

Table 3: FT synthesis results during first 12 hours.

% CO Conversion	FT synthesis rate (g CH/g cat/hr)	α	CO_2 selectivity	CH_4 selectivity	C_2-C_4 selectivity	C_{5+} selectivity
74.6	0.4192	0.86	1.2	13.7	5.4	79.7

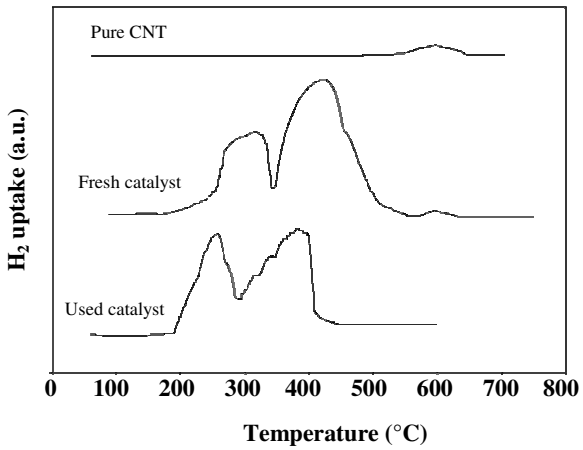

Fig. 8: TPR profile for the pure CNTs, calcined fresh and used 20wt%Co/CNT catalysts.

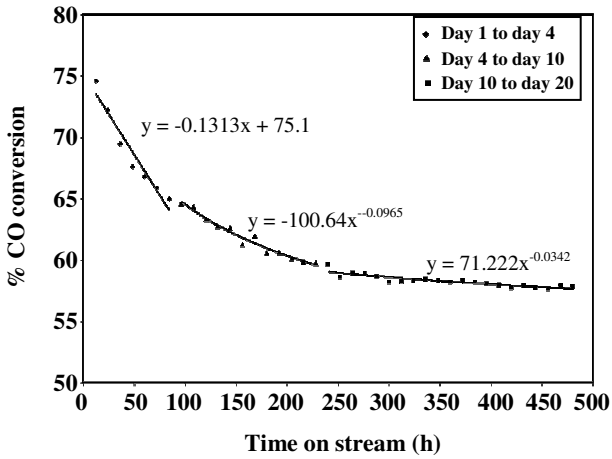

Fig. 9: %CO Conversion variations with time on stream ($T=220^oC$, $P=2$ MPa, $H_2/CO=2$).

supported cobalt based FT synthesis catalysts. However it's products distribution (13.7% CH_4, 5.4% C_2-C_4 and 79.7% C_{5+} selectivity) shows a slight shift to the lower molecular weight hydrocarbons. It is to note that the FT synthesis productivity of the commercial Al_2O_3, Si $O_2$and TiO_2 supported cobalt catalysts are 0.25-0.32g CH/ g cat./ h and the CH_4 and C_{5+} selectivities of the commercial catalysts are 4-6% and 86-93% respectively [23].

Fig. 9 presents the CO conversion changes with the duration of FT synthesis. As it can be seen, the %CO conversion sharply decreases in the first days, and then levels off. This Figure shows that a plateau region is reached after 10 days which indicates that the loss of active sites decreases significantly during the first 240 h of continues FT synthesis. Three different steps are distinguishable. The %CO conversion drops by 10% in the first 4 days while during the days 5-10 and 11-20 the %CO conversion only drops by 4.7% and 0.73%. The shape of declining curves of the first step, second step and third step deactivations are different. The deactivation curve sloped steeply at first and then moderately and finally very slowly. The loss of activity for the first deactivation step can be simulated with following linear correlation.

$$X_{CO} = -0.13T_{(hr)} + 75.1 \quad (9)$$

The linear deactivation mode suggests that the deactivation rate is zero order to CO conversion. This reveals that during first 4 days FT synthesis the deactivation rate is not related to the number of the catalyst active sites and the deactivation is caused by exterior factors [23]. It has been suggested that in FT synthesis on cobalt based catalysts at high conversions, the loss of active sites is caused by water-induced oxidation of cobalt [15-17,21,23]. This deactivation process entails cobalt redox transformation with no support participation. Another reason for this type of activity loss is the formation of more refractory forms of oxidized cobalt generated by cobalt-support interactions [21,23]. The extent of this type of deactivation also depends on the partial pressure of water produced during FT synthesis. It was recommended that water promotes interaction between cobalt oxide species and support [16,17]. So the larger deactivation observed for the first 4 days FT synthesis can be due to higher partial pressure of water as an exterior factor present in the catalytic bed of the reactor [15,16,17,21,23]. In other words, the results suggest that CNTs supported cobalt catalyst is more susceptible to re-oxidation and cobalt support interactions at higher partial pressures.

Thermodynamic studies on the stability of nanosized metallic cobalt crystallites in water/syngas mixtures show that, under realistic Fischer-Tropsch synthesis conditions the oxidation of bulk metallic cobalt is not feasible, unless the water partial pressure relative to the hydrogen and carbon monoxide partial pressures must be in excess of 50-60 [24]. However, the oxidation of small cobalt crystallites to Co(II)O or the formation of an oxide shell might be thermodynamically feasible under specific conditions. The stability of nanosized crystallites which are related to dispersion of cobalt particles, are dependent on the surface energy to the overall energy of the system that may vary with the crystallite size, morphology, the starting crystal phase, and the ratio of the partial pressure of water relative to the partial pressure of the syngas. It is shown that the spherical cobalt crystallites with a diameter less than 4.4 nm will not be stable thus leading to higher catalyst deactivation under industrially Fischer-Tropsch conditions [21,24]. The sharp decrease in percentage CO conversion during the first 4 days may come from the oxidation of these nanosized cobalt crystallites.

For the second and third deactivation steps, the catalyst deactivation could be simulated with power law expressions:

$$\text{Second step}: X_{CO} = 100.64 T_{(hr)}^{-0.0965} \quad (10)$$

$$\text{Third step}: X_{CO} = 71.22 T_{(hr)}^{-0.0342} \quad (11)$$

Assuming the deactivation rate is:

$$-\frac{dX}{dt} = kX^n \quad (12)$$

After integration and data reduction by least square fit, the power order (n) can be determined as 11.4 and 30.2 for the second and the third deactivation steps respectively. These values are in the range that ordinary metal catalysts would experience during sintering [25]. However the lower power order of 11.4 for the second deactivation step demonstrates that the rate of sintering during this step was significantly higher than that for the third step. The results of TEM tests showed that the rate of sintering of the particles located on the outer surfaces of the carbon nano tubes is higher than that of the particles located on the inner layers of the tubes. The zone with higher rate of sintering shown in Fig. 9 (step 2), can be assigned to the sintering of the particles located in the outer layers of the tubes and the zone with lower rate of sintering shown in this figure (step 3) can be attributed to the sintering of the particles located inside the tubes. The results of H_2 chemisorptions and re-oxidation tests showed in Table 2 confirm the cluster growth during 480 h reaction. FT synthesis temperature too is low to boost the cluster growth at the catalyst surface but it seems that water vapor increases the oxidation-reduction cycles on the catalyst surface which in turn leads to cluster growth or sintering. These results verify that to have a Co/CNTs catalyst with longer lifetime it is necessary to distribute the active metal particles in the inner layers of the carbon nano tubes. Decreasing the sintering rate of the cobalt particles which are located on the outer layer of the CNTs by introducing functional groups and defects that can act as anchoring sites for the cobalt particles, is one of the specific objectives of our current research program.

The regeneration of the used catalyst at 270°C increased %CO conversion from 57.9 to 63.5%. Also catalyst regeneration at 400°C increased the %CO conversion from 63.5 to 67.1%. The total activity recovery after the third regeneration step at 400°C (about 9.1%) is close to the total activity loss during the first deactivation step (about 10%). Since the catalyst deactivation due to sintering is an irreversible process, the activity recovery can be only assigned to the reduction of re-oxidized cobalts and reduction of cobalt species that interacted with support (step 1).

The uncondensed vapour stream of cold trap was reduced to atmospheric pressure through a pressure letdown valve. The composition of this stream was quantified using an on-line gas chromatograph. Also, the contents in hot and cold traps were removed every 24 h and the hydrocarbon and water fractions separated. The contents of these traps were then analyzed using a Varian CP 3400 GC equipped with a Petrocol Tmdh fused silica capillary column and a Flame Ionization Detector (FID) equipped in an offline GC. Fig. 10 shows the methane and C_5^+ liquid hydrocarbon selectivity variations with reaction time. This Figure displays that CH_4 selectivity decreases with time-on-stream during 480 h FT synthesis at 220°C and 2 MPa. Also, Fig. 10 shows that the C_{5+} selectivity increases during 480 h FT synthesis. It has been shown [26] that the larger cobalt particles are more selective to higher molecular weight hydrocarbons and

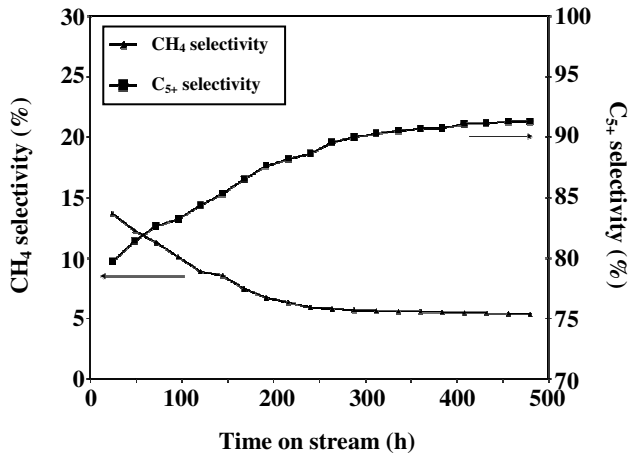

Fig. 10: Product selectivities variations with time on stream (T=220°C, P=2 MPa, $H_2/CO=2$).

smaller cobalt particles are selective to methane and light gaseous hydrocarbons. It can be concluded that sintering of the smaller particles leads to enhancement of C_{5+} selectivity and suppression of CH_4 production with time on stream.

As discussed earlier, higher rate of sintering of the particles located on the outer layers of the tubes increases the ratio of the particles located inside to the particles located on the outside layer of the tubes. Confinement of the reaction intermediates inside the pores can enhance their contact with cobalt particles, favouring the growth of longer chain hydrocarbons. In addition, the inner sides of the CNTs are electron deficient and can enhance the dissociation of CO resulting in production of higher chain hydrocarbons. Increasing the ratio of the particles located inside to the particles located on the outside layer of the tubes is believed to be the main reason for enhancement of C_{5+} selectivity and suppression of CH_4.

CONCLUSIONS

The results of this research reveal that the deposition of cobalt particles inside the carbon nano tubes pores improves the catalytic behaviour of the Co/CNT catalyst most likely due to difference in electronic properties of the inner and outer surface of the CNTs, and confinement effects. Sintering is the main source of irreversible deactivation in the CNTs supported cobalt FT synthesis catalysts. Due to the electron deficiency of the inner sides of the CNTs, the interaction between the cobalt oxides and the support is stronger leading to lower rates of sintering as compared with the particles located on the outer layers of the CNTs. Confinement of reaction intermediates inside the channels increases the contact time with active metal sites, resulting in production of heavier hydrocarbons. Another advantage of deposition of metal particles inside the pores is the physical encapsulation of metal particles which reduces the metal site sintering.

Abbreviations

FTS	Fischer-Tropsch Synthesis
TOS	Time on stream
BET	Brunauer, Emmett, and Teller
CNTs	Carbon nanotubes
XRD	X-ray diffraction
TPR	Temperature programmed reduction
ICP	Inductively coupled plasma
TEM	Transition electron microscopy
SEM	Scaning election microscopy
TPD	Temperature programmed desorption

Nomenclature

P	Pressure, MPa
T	Temperature, °C
%CO	Percent of CO conversion, mol%

Received : Jun. 23, 2009 ; Accepted : July 20, 2010

REFERENCES

[1] Tijmensen M.J.A., Faaij A.P.C., Hamelinck C.N., van Hardeveld M.R.M, Exploration of the Possibilities for Production of Fischer Tropsch Liquid and Power via Biomass Gasification, *Biomass and Bioenergy,* **23**, p. 129 (2002).

[2] Dry M.E., Fischer-Tropsch Reactions and the Environment, *Applied Catalysis A: General*, **189**, p. 185 (1999).

[3] Zhang J., Chen J., Ren J., Li Y., Sun Y., Support Effect of Co/Al_2O_3 Catalysts for Fischer-Tropsch Synthesis, *Fuel*, **82**, p. 581 (2003).

[4] Bukur D.B., Lang X., Mukesh D., Zimmerman W.H., Rosynek M. P., Li C., Binder/Support Effect on the Activity and Selectivity of Iron Catalysts in the Fisher-Tropsch Synthesis, *Ind. Eng. Chem. Res.*, **29**, p. 1588 (1990).

[5] Tavasoli A., Rashidi A.M., Sadaghiani Zadeh K., Karimi A., Kodadadi A., Mortazavi Y.A., Carbon Nano-Tube Supported Cobalt Catalyst for Converting Synthesis Gas to Hydrocarbons, European Patent EP1782885, (2005)

[6] Tavasoli A., Sadagiania K., Khorasheb F., Seifkordib A.A., Rohani A.A., Nakhaeipoura A., Cobalt Supported on Carbon Nanotubes-A Promising Novel Fischer-Tropsch Synthesis Catalyst, F*uel Proc. Tech*., **89**, p. 491 (2007).

[7] Tavasoli A., Nakhaeipour A., Irani M., Mortazavi Y., Khodadadi A., Dalai A., Preparation of Novel Super Active Fischer-Tropsch Cobalt Catalyst Supported on Carbon Nanotubes, *Iran. J. Chem. Chem. Eng.*, **28**(1), p. 37 (2009).

[8] Tavasoli A., Malek Abbaslou R.M., Mriane Trepanier, A. Dalai, Fischer-Tropsch Synthesis Over Cobalt Catalyst Supported on Carbon Nanotubes in a Slurry Reactor, *Appl. Catal. A: General,* **345**, p. 134 (2008).

[9] Malek Abbaslou R.M., Tavasoli A., Dalai A.K., Effect of Pre-Treatment on Physico-Chemical Properties and Stability of Carbon Nanotubes Supported Iron Fischer-Tropsch Catalysts, *Appl. Catal. A: General*, **355**, p. 33 (2009).

[10] Bezemer G.L., Bitter J.H., Kuipers, H.P.C.E., Oosterbeek H., Holewijn J.E., Xu X., Kapteijn F., van Dillen A.J., de Jong K.P., Cobalt Particle Size Effect in the Fischer-Tropsch Reaction Studied with Carbon Nanofiber Supported Catalysts, *J. Am. Chem. Soc.*, **128**, p. 3956 (2006).

[11] Ma W., Kugler E.L., Wright J., Dadyburjor D.B., Mo-Fe Catalysts Supported on Activated Carbon for Synthesis of Liquid Fuels by the Fischer-Tropsch Process: Effect of Mo Addition on Reducibility, Activity, and Hydrocarbon Selectivity, *Energy Fuels*, **20**, p. 2299 (2006).

[12] Guczi L., Stefler G., Geszti O., Koppány Zs., Kónya Z., Molnár É., Urbánc M., Kiricsi I., CO Hydrogenation Over Cobalt and Iron Catalysts Support Over Multi Wall Carbon Nanotubes: Effect of Preparation, *J. Catal.*, **244**, p. 24 (2006).

[13] Van Steen E., Prinsloo F.F., Some Evidence Refuting the Alkenyl Mechanism for Chain Growth in Iron-Based Fischer-Tropsch Synthesis, *Catal. Tod.*, **71**, p. 327 (2002).

[14] Serp P., Corrias M., Kalck P., Carbon Nanotubes and Nanofibers in Catalysis, *Appl. Catal. A: General*, **253**, p. 337 (2003).

[15] Tavasoli A., Nakhaeipour A., Sadaghiani K., Raising Co/Al_2O_3 Catalyst Lifetime in Fischer-Tropsch Synthesis by Using a Novel Dual-Bed Reactor, *Fuel proc. Tech.*, **88**, p. 461 (2007).

[16] Jacobs G., Patterson P.M., Das T., Luo M., Davis B., Fischer-Tropsch Synthesis: Effect of Water on Co/Al_2O_3 Catalysts and XAFS Characterization of Reoxidation Phenomena, *App. Catal. A: General*., **270**, p. 65 (2004).

[17] Jacobs G., Patterson P., Zhang Y., Das T., Li J., Davis B., Fischer-Tropsch Synthesis: Deactivation of Noble Metal-Promoted Co/Al_2O_3 Catalysts, *App. Catal.*, **233**, p. 215 (2002).

[18] Chen W., Pan X., Bao X., Tuning of Redox Properties of Iron and Iron Oxides via Encapsulation within Carbon Nanotubes, *J. Am. Chem. Soc.*, **129**, p. 7421 (2007).

[19] Pan X., Fan Z., Chen W., Ding Y., Luo H., Bao X., Effect of Confinement in Carbon Nanotubes on the Activity of Fischer-Tropsch Iron Catalyst, *Nature*, **6**, p. 507 (2007).

[20] Menon M., Andriotis A.N., Froudakis G.E., Anomalous Temperature Dependence of the Single Wall Carbon Nanotubes Resistivity, *Phys Lett.*, **320**, p. 425 (2000).

[21] Tavasoli A., Malek Abbaslou R.M., Dalai A., Deactivation Behavior of Ruthenium Promoted $Co/\gamma\text{-}Al_2O_3$ Catalysts in Fischer-Tropsch Synthesis, *Appl. Catal. A: General*, **346**, p. 58 (2008).

[22] Trepanier, M. Tavasoli A., Dalai A., Co, Ru and K Loadings Effects on the Activity and Selectivity of Carbon Nanotubes Supported Cobalt Catalyst in Fischer-Tropsch Synthesis, *Appl Catal. A: General*, **353**, p. 193 (2009).

[23] Tavasoli A., Irani M., Malek Abbaslou R.M., Tr´epanier M., Dalai A., Morphology and Deactivation Behavior of $Co\text{-}Ru/\gamma\text{-}Al_2O_3$ Fischer-Tropsch Synthesis Catalyst, *Can. J. Chem. Eng.*, **86**(6), p. 1070 (2008).

[24] van Steen E., Claeys M., Dry M.E., van de Loosdrecht J., Visagie E.L., Stability of Nanocrystals: Thermodynamic Analysis of Oxidation and Re-Reduction of Cobalt in Water/Hydrogen Mixture, *J. Phys. Chem. B*, **109**, p. 3575 (2005).

[25] Bartholomew C.H., Mechanism of Catalyst Deactivation, *Appl. Catal. A: General*, **212**, p. 17 (2001).

[26] Tavasoli A., Sadaghiani K., Nakhaeipour A., Ahangari M.G., Cobalt Loading Effects on the Structure and Activity for Fischer-Tropsch and Water-Gas Shift Reactions of Co/Al_2O_3 Catalysts, *Iran. J. Chem. Chem. Eng.*, **26**(1), p. 1 (2007).